# Cooperative Maximum Likelihood Target Position Estimation for MIMO-ISAC Networks

Lorenzo Pucci, Member, IEEE, Tommaso Bacchielli, Graduate Student Member, IEEE, and Andrea Giorgetti, Senior Member, IEEE

Abstract—This letter investigates target position estimation in integrated sensing and communication networks composed of multiple cooperating monostatic base stations (BSs). Each BS employs a MIMO-orthogonal time-frequency space (OTFS) scheme, enabling the coexistence of communication and sensing. A general cooperative maximum likelihood (ML) framework is derived, directly estimating the target position in a common reference system rather than relying on local range and angle estimates at each BS. Positioning accuracy is evaluated in single-target scenarios by varying the number of collaborating BSs, using root mean square error (RMSE), and comparing against the square root of the Cramér-Rao lower bound. Numerical results demonstrate that the ML framework significantly reduces the position RMSE as the number of cooperating BSs increases.

Index Terms—ISAC, cooperative sensing, maximum likelihood, Cramér-Rao lower bound, OTFS.

#### I. INTRODUCTION

THE marriage of integrated sensing and communication (ISAC) and mobile networks unlocks sensing capabilities not yet available, while also facilitating cooperative multibase stations (BSs) strategies that have proven effective for improved localization and tracking [1]. Recent studies have examined BS selection and resource allocation in cooperative ISAC systems [2]-[6], yet tracking high-speed targets (e.g., autonomous vehicles) remains challenging under severe Doppler effects and rapidly changing environments. Among candidate waveforms, orthogonal time frequency space (OTFS) modulation is robust to Doppler shifts and maps time-varying channels to the delay-Doppler domain, making it well-suited for ISAC [7]. Fully exploiting these advantages requires processing frameworks that leverage the spatial diversity inherent in cooperative multi-BSs systems. However, a key challenge persists in deriving a closed-form expression for cooperative maximum likelihood (ML) target position estimation from jointly processed signals at multiple BSs.

To address this, we propose an OTFS-based cooperative ISAC system with multiple monostatic multiple-input

© 2025 IEEE. Personal use of this material is permitted. Permission from IEEE must be obtained for all other uses, in any current or future media, including reprinting/republishing this material for advertising or promotional purposes, creating new collective works, for resale or redistribution to servers or lists, or reuse of any copyrighted component of this work in other works. DOI: 10.1109/LWC.2025.3548446.

This work was supported by the European Union - Next Generation EU under the Italian National Recovery and Resilience Plan (NRRP), Mission 4, Component 2, Investment 1.3, partnership on "Telecommunications of the Future" (PE00000001 - program "RESTART"). The authors are with the Wireless Communications Laboratory, CNIT, DEI, University of Bologna, Italy, Email: {lorenzo.pucci3, tommaso.bacchielli2, andrea.giorgetti}@unibo.it

multiple-output (MIMO) BSs and a general ML framework for target position estimation. Specifically, in the proposed framework, signals from each BS are processed at a fusion center to estimate the target position relative to a common reference system. Additionally, we derive the Cramér-Rao lower bound (CRLB) for position estimation in the proposed cooperative system, whose square root, the position error bound (PEB), provides a theoretical lower bound on accuracy. Numerical results demonstrate that BS cooperation based on ML estimation significantly improves localization accuracy—often achieving multi-fold improvements compared to single BS configurations—and validate the ML estimation against the PEB.

In this letter, capital and lowercase bold letters denote matrices and vectors. The operators  $(\cdot)^T$ ,  $(\cdot)^H$ ,  $\mathrm{Tr}(\cdot)$ , and  $\|\cdot\|$  refer to the transpose, conjugate transpose, trace, and Euclidean norm;  $\{a_i\}_{i=1}^N$  denotes a vector  $\mathbf{a} = [a_1,\ldots,a_N]$  and  $\mathbf{I}_n$  is the  $n \times n$  identity matrix;  $\mathbb{E}\{\cdot\}$  and  $\mathbb{V}\{\cdot\}$  denote the mean value and variance;  $\mathbf{x} \sim \mathcal{CN}(\mathbf{0}, \mathbf{\Sigma})$  represents a zero-mean circularly symmetric complex Gaussian vector with covariance  $\mathbf{\Sigma}$ . Additionally,  $\mathfrak{Re}(\cdot)$ ,  $|\cdot|$ , and  $\angle(\cdot)$  denote the real part, the absolute value, and the argument of a (real or complex) number, and  $\otimes$  represents the Kronecker product.

The letter is organized as follows: Section II introduces the system model, Section III outlines the cooperative ML estimation framework and the CRLB, Section IV presents numerical results, and Section V concludes the paper.

#### II. SYSTEM MODEL

# A. Physical Model

We consider an OTFS-based network, where monostatic BSs, each equipped with an ISAC transceiver with  $N_{\rm T}$  transmit and  $N_{\rm R}$  receive antennas, cooperate through a fusion center to localize targets within a designated region, as shown in Fig. 1. Each BS can split sensing and communication in a time- or frequency-division manner based on the required quality of service.  $^{1}$ 

The network operates at a carrier frequency  $f_{\rm c}$ , with a bandwidth  $B=M\Delta f\ll f_{\rm c}$ , where M is the number of subcarriers and  $\Delta f=1/T$  is the subcarrier spacing, with T being the time slot duration. Consider a scenario with P point-like targets, each moving with a radial velocity  $v_p$  at a distance  $r_p$  from the monostatic transceiver and with radar cross-section

<sup>1</sup>Interference between BSs can be mitigated using frequency and time division approaches, possibly complemented by dynamic resource allocation methods such as dynamic frequency reuse and inter-cell resource sharing [8].

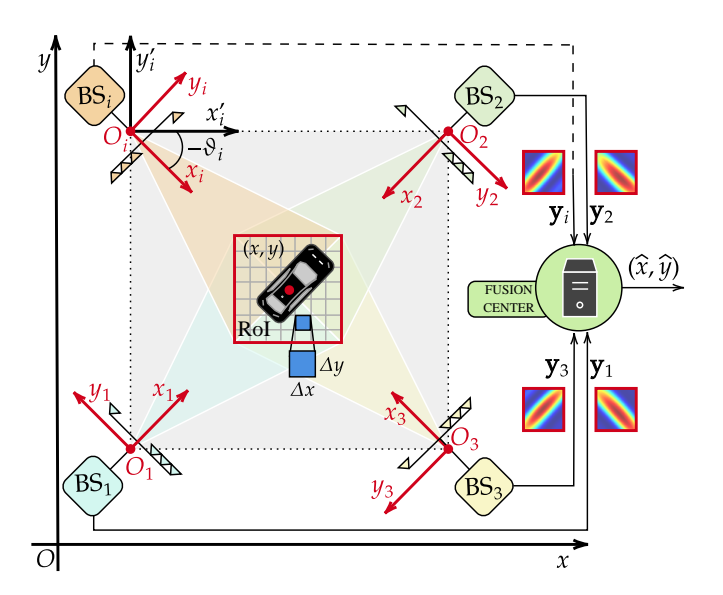


Fig. 1. Network of  $N_{\rm bs}$  cooperating BSs for target localization. The red square marks the RoI considered for fine-grained grid-based ML estimation.

(RCS)  $\sigma_p$ . Assuming far-field line of sight (LoS) propagation between the transceiver and each target, the  $N_{\rm R} \times N_{\rm T}$  complex baseband channel impulse response of the radar function is

$$\mathbf{H}(t,\tau) = \sum_{p=0}^{P-1} \alpha_p \mathbf{b}(\phi_p) \mathbf{a}^{\mathsf{H}}(\phi_p) \delta(\tau - \tau_p) e^{j2\pi f_{\mathrm{D},p}t}$$
(1)

where  $\alpha_p$  is the complex channel gain, accounting for attenuation and phase shift,  $f_{\mathrm{D},p}=2v_pf_c/c$  represents the Doppler shift, and  $\tau_p=2r_p/c$  is the round-trip delay, with c denoting the speed of light. According to the radar equation,  $|\alpha_p|^2=\frac{G^2\sigma_p\,c^2}{(4\pi)^3\,f_c^2\,r_p^4}$ , where  $G^2$  accounts for the single antenna element gain G of the transmitter (Tx) and receiver (Rx) arrays. Furthermore,  $\mathbf{a}(\phi_p)$  and  $\mathbf{b}(\phi_p)$  denote the Tx and Rx array response vectors associated with the p-th target, with  $\phi_p$  the p-th angle of departure (AoD)/angle of arrival (AoA), assumed to be equal in the monostatic setup. For uniform linear arrays (ULAs) with  $N_{\mathrm{T}}$  antenna elements spaced at half-wavelength intervals, the array response vector is given by  $\mathbf{a}(\phi_p)=[e^{-j\frac{N_{\mathrm{T}}-1}{2}\pi\sin\phi_p},\ldots,e^{j\frac{N_{\mathrm{T}}-1}{2}\pi\sin\phi_p}]^{\mathrm{T}}$ . The same definition applies to  $\mathbf{b}(\phi_p)$  with  $N_{\mathrm{R}}$ .

#### B. OTFS-ISAC Input-Output Relationship

Considering a total of N time slots, the vector of signals transmitted through the  $N_{\rm T}$  antennas at the n-th time slot is

$$\mathbf{s}_n(t) = \sqrt{P_{\text{avg}}} \sum_{m=0}^{M-1} X[n, m] \mathbf{w}_{\text{T}} e^{j2\pi m\Delta f(t-nT)} g_{\text{tx}}(t - nT)$$
(2)

where  $P_{\mathrm{avg}} = P_{\mathrm{T}}/M$  is the average transmit power per subcarrier with  $P_{\mathrm{T}}$  the total transmit power dedicated to sensing. The vector  $\mathbf{w}_{\mathrm{T}}$  represents the unit-norm beamforming vector, chosen to provide nearly constant gain over a given circular sector, following the approach outlined in [9]. The pulse shape is represented by  $g_{\mathrm{tx}}(t)$  and  $X[n,m] \in \mathbb{C}$  is the complex symbol located in the  $N \times M$  time-frequency

domain grid obtained via symplectic finite Fourier transform (SFFT) from complex data symbols  $x[k,l] \in \mathcal{A}$ , where  $\mathcal{A}$  is the complex alphabet and  $\mathbb{E}\{|x[k,l]|^2\}=1$ , arranged in the  $M \times N$  delay-Doppler domain grid, i.e.,

$$X[n,m] = \frac{1}{\sqrt{NM}} \sum_{k=0}^{M-1} \sum_{l=0}^{N-1} x[k,l] e^{-j2\pi(\frac{mk}{M} - \frac{nl}{N})}$$
 (3)

with n, l = 0, ..., N - 1 and m, k = 0, ..., M - 1. Further details on the processing chain are available in [7], [10], [11].

The transmitted signal  $\{s_n(t)\}_{n=0}^{N-1}$ , after the channel (1), is collected at each Rx antenna and processed by a filter matched to the demodulating pulse  $g_{\rm rx}(t)$ . In the ideal case of bi-orthogonality between transmitting and receiving pulses for integer multiples of T and  $\Delta f$ , inter-symbol interference (ISI) can be avoided without a cyclic prefix (CP). However, in the more realistic scenario of imperfect bi-orthogonality, as considered here, some residual ISI occurs without a CP [10]. The output of the matched filter is then sampled at t = nT and  $f = m\Delta f$ , forming a  $N \times M$  symbol grid in the time-frequency domain, whose (n,m) element is [10]

$$Y[n,m] = \sum_{n'=0}^{N-1} \sum_{m'=0}^{M-1} X[n',m'] \mathbf{h}_{n,m}[n',m']$$
 (4)

where  $\mathbf{h}_{n,m}[n',m']$  is the  $N_{\mathrm{R}} \times 1$  channel vector in the time-frequency domain. Without loss of generality, we focus on one target, i.e., P=1 in (1), so the index p is dropped and the channel vector becomes

$$\mathbf{h}_{n,m}[n',m'] = (5)$$

$$h\mathbf{b}(\phi)e^{j2\pi(n'Tf_{D}-m\Delta f\tau)}A_{g_{r},g_{t}}(\tau_{n,n'},f_{D,m,m'})$$

where  $h \triangleq \sqrt{P_{\mathrm{avg}}} \gamma \alpha \, e^{j2\pi f_{\mathrm{D}}\tau}$  is the overall complex channel factor, being  $\gamma = \mathbf{a}^{\mathrm{H}}(\phi)\mathbf{w}_{\mathrm{T}}$  the complex beamforming factor related to the AoD of the target,  $\tau_{n,n'} = (n-n')T-\tau$ , and  $f_{\mathrm{D},m,m'} = (m-m')\Delta f - f_{\mathrm{D}}$ . The term  $A_{g_{\mathrm{r}},g_{\mathrm{t}}}\left(\tau_{n,n'},f_{\mathrm{D},m,m'}\right)$  is the cross-ambiguity function, in the delay-Doppler domain, between the two pulses  $g_{\mathrm{r}}(t)$  and  $g_{\mathrm{t}}(t)$ , here both chosen to be rectangular of duration  $T^2$ . Lastly, the demodulated symbols, back in the delay-Doppler domain, can be obtained by performing inverse symplectic finite Fourier transform (ISFFT) on the symbols in (4), as  $\mathbf{y}[k,l] = h\mathbf{b}(\phi)\sum_{k'=0}^{M-1}\sum_{l'=0}^{N-1}x[k',l']\Psi_{l,l'}[k,k']$ , where  $\Psi_{l,l'}[k,k']$  is the (l,l',k,k') complex element of the matrix  $\mathbf{\Psi} \in \mathbb{C}^{MN \times MN}$ , which retains information on Doppler shift and round-trip delay for the target, defined as

$$\Psi_{l,l'}[k,k'] = \frac{1}{NM} \sum_{n,n',m,m'} \Lambda_{n,n',m,m'} A_{g_{r},g_{t}}(\tau_{n,n'}, f_{D,m,m'})$$

where  $\Lambda_{n,m,n',m'}=e^{j2\pi\left(n'Tf_{\rm D}-m\Delta f\tau-\frac{nl-n'l'}{N}+\frac{mk-m'k'}{M}\right)}$ . Under the hypothesis of rectangular pulses and a maximum

<sup>2</sup>The cross-ambiguity function between two generic pulses  $g_u(t)$  and  $g_v(t)$  of duration T is defined as [7]

$$A_{g_u,g_v}(\tau, f_{\mathrm{D}}) \triangleq \int_0^T g_u(t)g_v^*(t-\tau)e^{-j2\pi f_{\mathrm{D}}t}dt.$$

3

channel delay smaller than T, an easy-to-handle expression of this matrix's elements can be found in [7], [11].

Through a vectorization operation performed on the transmitted symbols x[k,l], the input-output relationship can be written compactly as

$$\mathbf{y} = h\mathbf{G}(f_{\mathrm{D}}, \tau, \phi)\mathbf{x} + \boldsymbol{\nu} \tag{6}$$

where  $\mathbf{y} \in \mathbb{C}^{MNN_{\mathrm{R}} \times 1}$  contains the received symbols at each Rx antenna,  $\mathbf{G}(f_{\mathrm{D}}, \tau, \phi) \triangleq \mathbf{b}(\phi) \otimes \mathbf{\Psi} \in \mathbb{C}^{MNN_{\mathrm{R}} \times MN}$  is the effective channel matrix [12],  $\boldsymbol{\nu} \sim \mathcal{CN}(\mathbf{0}_{MNN_{\mathrm{R}}}, \sigma_{\nu}^2 \mathbf{I}_{MNN_{\mathrm{R}}})$  is the complex additive white Gaussian noise (AWGN) vector with  $\sigma_{\nu}^2 = N_0 \Delta f$ , with  $N_0$  the noise power spectral density (PSD).

# III. SENSING PARAMETERS ESTIMATION AND CRAMÉR-RAO LOWER BOUND

#### A. Cooperative Maximum Likelihood Position Estimation

Let us consider the scenario in Fig. 1, where  $N_{\rm bs}$  BSs at coordinates  $\mathcal{O}_i = [x_{\rm bs}^{(i)}, y_{\rm bs}^{(i)}]^{\sf T}$ , with  $i=1,\ldots,N_{\rm bs}$ , cooperate to locate the point-like target at  $\mathbf{p}=[x,y]^{\sf T}$  in a common Cartesian reference system. The target position in the local reference system centered at  $\mathcal{O}_i$  is given by  $\mathbf{p}_i = [x_i,y_i]^{\sf T} = [r_i\cos(\phi_i),r_i\sin(\phi_i)]^{\sf T}$ , with  $r_i=\tau_i\,c/2$ .

By collecting the backscattered signals by the *i*-th BS,  $\mathbf{y}_i$ , detailed in (6), the vector  $\tilde{\mathbf{y}} \in \mathbb{C}^{MNN_{\mathrm{R}}N_{\mathrm{bs}}\times 1}$  of all received symbols is

$$\tilde{\mathbf{y}} = \begin{bmatrix} \mathbf{y}_1^\mathsf{T}, \mathbf{y}_2^\mathsf{T}, \dots, \mathbf{y}_{N_{\mathrm{bs}}}^\mathsf{T} \end{bmatrix}^\mathsf{T}.$$
 (7)

The vector of target parameters to be estimated with respect to the *i*-th BS is  $\boldsymbol{\theta}_i = [\beta_i, \varphi_i, f_{\mathrm{D},i}, \tau_i, \phi_i]^\mathsf{T}$ , where  $\beta_i = |h_i|$  and  $\varphi_i = \angle h_i$ , and the complete set of unknown parameters is indicated with  $\boldsymbol{\Theta} = \begin{bmatrix} \boldsymbol{\theta}_1^\mathsf{T}, \boldsymbol{\theta}_2^\mathsf{T} \cdots, \boldsymbol{\theta}_{N_{\mathrm{bs}}}^\mathsf{T} \end{bmatrix}^\mathsf{T} \in \Gamma$ , where  $\Gamma = \mathbb{C}^{N_{\mathrm{bs}}} \times \mathbb{R}^{3N_{\mathrm{bs}}}$  is the considered parameter space.

Ignoring the terms that are not relevant for the estimation, the log-likelihood function of the received signal in (7) is

$$l(\tilde{\mathbf{y}}; \boldsymbol{\Theta}, \mathbf{x}) \approx -\frac{1}{\sigma_{\nu}^{2}} \sum_{i=1}^{N_{\text{bs}}} \left\| \mathbf{y}_{i} - h_{i} \mathbf{G}(f_{\text{D},i}, \tau_{i}, \phi_{i}) \mathbf{x}_{i} \right\|^{2}.$$
(8)

From (8), an ML estimation problem can be formulated to estimate the unknown parameters in  $\Theta$ , as follows

$$\widehat{\mathbf{\Theta}}_{\mathrm{ML}} = \underset{\mathbf{\Theta} \in \Gamma}{\mathrm{arg\,max}} \ l(\tilde{\mathbf{y}}; \mathbf{\Theta}, \mathbf{x}). \tag{9}$$

Notably, the estimate of each complex channel coefficient  $h_i$  depends solely on the received signal  $\mathbf{y}_i$  at the i-th BS. Under this premise, the ML estimator of the i-th channel coefficient,  $\widehat{h}_i$ , is given by (21) in the Appendix. By substituting  $\widehat{h}_i$  into (8) and applying the same steps as outlined in the Appendix, (9) can be rewritten as

$$\{\widehat{f}_{\mathrm{D},i},\widehat{\tau}_{i},\widehat{\phi}_{i}\}_{i=1}^{N_{\mathrm{bs}}} = \underset{\{f_{\mathrm{D},i},\tau_{i},\phi_{i}\}_{i=1}^{N_{\mathrm{bs}}} \in \Omega}{\arg\max} \sum_{i=1}^{N_{\mathrm{bs}}} \frac{|\mathbf{y}_{i}^{\mathsf{H}}\mathbf{G}(f_{\mathrm{D},i},\tau_{i},\phi_{i})\mathbf{x}_{i}|^{2}}{\|\mathbf{G}(f_{\mathrm{D},i},\tau_{i},\phi_{i})\mathbf{x}_{i}\|^{2}}$$
(10)

where  $\Omega = \mathbb{R}^{3N_{\rm bs}}$  is the search space. The ML estimation in (10) can be further simplified as derived below.

TABLE I JSC NETWORK PARAMETERS

Parameters	Symbols	Values
Number of Tx and Rx antennas	$N_{\rm T}$ , $N_{\rm R}$	16
Antenna element gain	G	1
Tx beamwidth / Beamforming gain	BW $/  \gamma ^2$	$40^{\circ}$ / $\sim 4.1$ dB
Total transmit power	$P_{\mathrm{T}}$	30 dBm
Carrier frequency	$f_{\rm c}$	60 GHz
Time slots / Active subcarriers	N/M	50 / 96
Subcarrier spacing / Time slot duration	$\Delta f / T$	1 MHz / 1 μs
Noise PSD / Target RCS	Ν <sub>0</sub> / σ	4 · 10 <sup>-20</sup> W/Hz / 1 m <sup>2</sup>
Region-of-interest / pixel size	RoI / $(\Delta x \times \Delta y)$	$16 \text{ m}^2 \text{ / } (0.02 \times 0.02) \text{ m}^2$

Referring to Fig. 1, the relationship between  $\mathbf{p}_i$  and  $\mathbf{p}$  is given by the following transformation

$$\{x_i = x_i' \cos(\vartheta_i) + y_i' \sin(\vartheta_i); y_i = -x_i' \sin(\vartheta_i) + y_i' \cos(\vartheta_i)\}$$
(11)

where  $x_i' = x - x_{\rm bs}^{(i)}$  and  $y_i' = y - y_{\rm bs}^{(i)}$ , while  $\vartheta_i$  is the counterclockwise rotation angle of the *i*-th reference system with respect to the common one. The local coordinates of the target,  $\mathbf{p}_i$ , are in turn related to the unknown parameters  $(\tau_i, \phi_i)$ , through

$$\left\{ \phi_i = \arctan(y_i/x_i); \ \tau_i = \frac{2}{c} \sqrt{x_i^2 + y_i^2} \right\}.$$
 (12)

Therefore, the parameters  $\{\tau_i, \phi_i\}_{i=1}^{N_{\rm bs}} \subset \Theta$  can be expressed as a function of the target position  $\mathbf{p}$  in the common reference system, i.e.,  $\{\tau_i(\mathbf{p}), \phi_i(\mathbf{p})\}_{i=1}^{N_{\rm bs}}$ . The ML estimator in (10) can then be rewritten as

$$\left[\widehat{f}_{\mathrm{D},1},\dots,\widehat{f}_{\mathrm{D},N_{\mathrm{bs}}},\widehat{\mathbf{p}}\right] = \tag{13}$$

$$= \underset{\left[\left\{f_{\mathrm{D},i}\right\}_{i=1}^{N_{\mathrm{bs}}},\mathbf{p}\right] \in \Pi}{\arg\max} \sum_{i=1}^{N_{\mathrm{bs}}} \frac{|\mathbf{y}_{i}^{\mathsf{H}}\mathbf{G}(f_{\mathrm{D},i},\tau_{i}(\mathbf{p}),\phi_{i}(\mathbf{p}))\mathbf{x}_{i}|^{2}}{\left\|\mathbf{G}(f_{\mathrm{D},i},\tau_{i}(\mathbf{p}),\phi_{i}(\mathbf{p}))\mathbf{x}_{i}\right\|^{2}}$$

with  $\Pi = \mathbb{R}^{N_{\rm bs}+2}$  the new search space.

Lastly, if for a given  $\mathbf{p}$ , or  $(\tau_i,\phi_i)$  pair, the estimate of the Doppler shift,  $\widehat{f}_{\mathrm{D},i}$ , can be computed at each BS (e.g., through a coarse estimation procedure or by exploiting information from tracking algorithms) and then replaced in (13), the cooperative ML target position estimation for an ISAC network composed of  $N_{\mathrm{bs}}$  BS can be computed as

$$\widehat{\mathbf{p}} = \underset{\mathbf{p} \in \mathbb{R}^2}{\arg \max} \sum_{i=1}^{N_{\text{bs}}} \frac{|\mathbf{y}_i^{\mathsf{H}} \mathbf{G}(\widehat{f}_{\mathrm{D},i}, \tau_i(\mathbf{p}), \phi_i(\mathbf{p})) \mathbf{x}_i|^2}{\|\mathbf{G}(\widehat{f}_{\mathrm{D},i}, \tau_i(\mathbf{p}), \phi_i(\mathbf{p})) \mathbf{x}_i\|^2}.$$
 (14)

Interestingly, (14) also applies to orthogonal frequency-division multiplexing (OFDM), where the effective channel matrix **G** can be represented as in [13, Equation (23)].

#### B. Numerical Evaluation of Cooperative Maximum Likelihood

As mentioned, solving (14) requires an initial estimation of the Doppler shifts  $\{f_{\mathrm{D},i}\}_{i=1}^{N_{\mathrm{bs}}}$ , achieved by evaluating (10) within the defined search space  $\Omega$ . For a cooperative ISAC system with  $N_{\mathrm{bs}} \geq 2$  BSs, this ML estimation operates in a continuous search space of dimension  $\geq 6$ , leading to considerable complexity. To simplify computation, we employ an approximate method: breaking down the estimation into  $N_{\mathrm{bs}}$  independent problems, each in a 3D search space  $\tilde{\Omega} \subset \Omega$ .

Assuming a prior target detection phase has identified a RoI as in [13], the search space for  $\{\tau_i,\phi_i\}_{i=1}^{N_{\rm bs}}$  in (10) is limited to range of values within the RoI (see Fig. 1). Doppler shifts  $\{f_{{\rm D},i}\}_{i=1}^{N_{\rm bs}}$  are similarly restricted, based on the scenario. Hence, we define a discrete set of tuples  $(f_{{\rm D},i},\tau_i,\phi_i)\in\tilde{\Omega}$  as

$$\tilde{\Omega} = \{f_{\text{D}i}^{\text{min}}, ..., f_{\text{D}i}^{\text{max}}\} \times \{\tau_i^{\text{min}}, ..., \tau_i^{\text{max}}\} \times \{\phi_i^{\text{min}}, ..., \phi_i^{\text{max}}\}$$

with steps  $\delta f_{\rm D}=c_{f_{\rm D}}\Delta f_{\rm D},\ \delta \tau=c_{\tau}\Delta \tau,\ {\rm and}\ \delta \phi=c_{\phi}\Delta \Phi,\ {\rm being}\ \Delta f_{\rm D}=1/(NT)\ {\rm and}\ \Delta \tau=1/(M\Delta f)\ {\rm the}\ {\rm system}\ {\rm resolution}\ {\rm in}\ {\rm Doppler}\ {\rm and}\ \Delta \Phi=1/(M\Delta f)\ {\rm the}\ {\rm system}\ {\rm resolution}\ {\rm in}\ {\rm Doppler}\ {\rm and}\ \Delta \Phi=1/(M\Delta f)\ {\rm the}\ {\rm system}\ {\rm resolution}\ {\rm in}\ {\rm Doppler}\ {\rm and}\ \Delta \Phi$  the beamwidth at 0 degrees. Moreover,  $c_{f_{\rm D}},c_{\tau},c_{\phi}\in(0,1]$  are factors used to control the desired accuracy of parameter estimation. Once Doppler shifts  $\{\widehat f_{\rm D,i}\}_{i=1}^{N_{\rm bs}}$  are estimated, (14) can then be used to compute  $\widehat p$ . As before, the search is discretized within the RoI by defining a discrete set of common coordinates as  $\{x_{\rm min},...,x_{\rm max}\}\times\{y_{\rm min},...,y_{\rm max}\}$ , with steps  $\Delta x$  and  $\Delta y$ , respectively, chosen to achieve the desired accuracy. Notably, (14) can be interpreted as a summation of  $N_{\rm bs}$  radar maps in the x-y plane, computed within the RoI, as shown in Fig. 1.

#### C. Cramér-Rao Lower Bound Derivation

This section derives the CRLB, the fundamental lower limit on the variance of unbiased estimators, specifically for target position estimation.

Let  $\mu_i = h_i \mathbf{G}(f_{D,i}, \tau_i, \phi_i) \mathbf{x}_i \in \mathbb{C}^{MNN_R \times 1}$  be the vector of mean values of the received signal  $\mathbf{y}_i$  at the *i*-th BS. For the vector of unknown parameters  $\boldsymbol{\theta}_i$ , the CRLB is given by

$$\mathbb{V}\{\hat{\theta}_{i,q}\} \geq \mathrm{CRLB}(\theta_{i,q}) = \left[\boldsymbol{\mathcal{I}}^{-1}(\boldsymbol{\theta}_i)\right]_{q,q} \ q = 1, \dots, \mathrm{card}(\boldsymbol{\theta}_i)$$

where  $\hat{\theta}_{i,q}$  is the estimate of the q-th parameter contained in  $\theta_i$ , and  $[\mathcal{I}^{-1}(\theta_i)]_{q,q}$  represents the q-th element on the main diagonal of the inverse of the Fisher information matrix (FIM)  $\mathcal{I}(\theta_i)$ . The vector  $\mu_i$  can be reshaped into a 3D array with elements  $\mu_i[k,l,j]$ , indexed by (k,l,j), corresponding to dimensions  $(M\times N\times N_{\mathrm{R}})$ , respectively. The generic qp-th element of  $\mathcal{I}(\theta_i)$  can then be computed as [11]

$$\left[\mathcal{I}(\boldsymbol{\theta}_{i})\right]_{q,p} = \frac{2}{\sigma_{\nu}^{2}} \mathfrak{Re} \left\{ \sum_{k,l,j} \left( \frac{\partial \mu_{i}[k,l,j]}{\partial \theta_{i,q}} \right)^{*} \left( \frac{\partial \mu_{i}[k,l,j]}{\partial \theta_{i,p}} \right) \right\} \tag{15}$$

where

$$\mu_i[k,l,j] = \beta_i e^{j\varphi_i} b_j(\phi_i) \sum_{k'=0}^{M-1} \sum_{l'=0}^{N-1} \Psi_{l,l'}[k,k'] x_i[k',l'] \quad (16)$$

with  $b_j(\phi)$  the j-th element of the array response vector  $\mathbf{b}(\phi)$ . The vector  $\boldsymbol{\theta}_i$  can be partitioned as  $\boldsymbol{\theta}_i = [\boldsymbol{\theta}_{i,1}^\mathsf{T}, \boldsymbol{\theta}_{i,2}^\mathsf{T}]^\mathsf{T}$ , with  $\boldsymbol{\theta}_{i,1} = [\beta_i, \varphi_i, f_{\mathrm{D},i}]^\mathsf{T}$ ,  $\boldsymbol{\theta}_{i,2} = [\tau_i, \phi_i]^\mathsf{T}$ , which induces the partition of the FIM into the matrices  $\mathbf{A} \in \mathbb{R}^{3\times3}$ ,  $\mathbf{B} \in \mathbb{R}^{3\times2}$ , and  $\mathbf{C} \in \mathbb{R}^{2\times2}$ , as  $\mathcal{I}(\boldsymbol{\theta}_i) = \begin{bmatrix} \mathbf{A} & \mathbf{B} \\ \mathbf{B}^\mathsf{T} & \mathbf{C} \end{bmatrix}$ . Then, the equivalent Fisher information (EFIM) is [15], [16]:  $\mathcal{I}_{\mathbf{e}}(\boldsymbol{\theta}_{i,2}) = \mathbf{C} - \mathbf{B}^\mathsf{T} \mathbf{A}^{-1} \mathbf{B}$ .

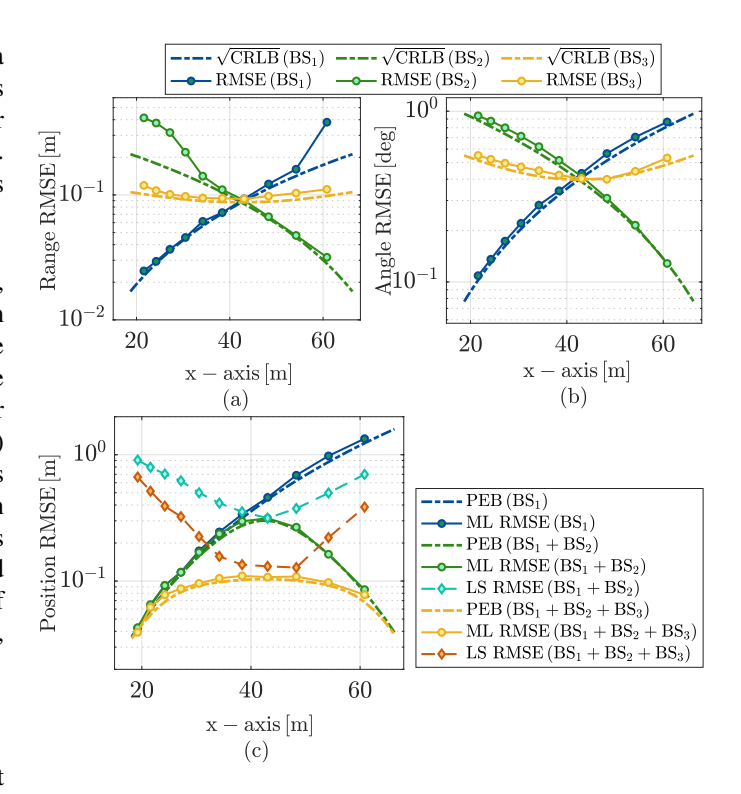


Fig. 2. RMSE and  $\sqrt{\text{CRLB}}$  for estimates of range  $\hat{r}$  (a), angle  $\hat{\phi}$  (b), and position  $\hat{\mathbf{p}}$  (c) as the target moves along the diagonal line between BS<sub>1</sub> and BS<sub>2</sub> within the square area shown in Fig. 1. The *x*-axis represents the target's position – in the common reference system – along the diagonal, where y=x.

Considering that each BS independently observes the target parameters, the FIM for cooperative position estimation is given by [15], [16]:  $\mathcal{I}_{\rm e}(\mathbf{p}) = \sum_{i=1}^{N_{\rm BS}} \mathbf{J}_{\rm n}^{\sf T} \Big( \mathbf{J}_{\rm m}^{\sf T} \mathcal{I}_{\rm e}(\boldsymbol{\theta}_{i,2}) \mathbf{J}_{\rm m} \Big) \mathbf{J}_{\rm n}$ , where  $\mathbf{J}_{\rm m}$  and  $\mathbf{J}_{\rm n}$  represent the Jacobian of the transformations  $\mathbf{p}_i \to (\tau_i, \phi_i)$ , and  $\mathbf{p} \to \mathbf{p}_i$ , respectively, whose definition, considering (12) and (11), are as follows

$$\mathbf{J}_{\mathbf{m}} \triangleq \begin{bmatrix} \frac{\partial \tau_{i}}{\partial x_{i}} & \frac{\partial \tau_{i}}{\partial y_{i}} \\ \frac{\partial \phi_{i}}{\partial x_{i}} & \frac{\partial \phi_{i}}{\partial y_{i}} \end{bmatrix}, \qquad \mathbf{J}_{\mathbf{n}} \triangleq \begin{bmatrix} \frac{\partial x_{i}}{\partial x} & \frac{\partial x_{i}}{\partial y} \\ \frac{\partial y_{i}}{\partial x} & \frac{\partial y_{i}}{\partial y_{i}} \end{bmatrix}. \tag{17}$$

After computing (17), the CRLB of position estimate is determined as  $\mathbb{V}\{\hat{\mathbf{p}}\} \geq \mathrm{CRLB}(\mathbf{p}) = \mathrm{Tr}(\mathcal{I}_{\mathrm{e}}^{-1}(\mathbf{p}))$ . The PEB is then defined as  $\mathrm{PEB} \triangleq \sqrt{\mathrm{CRLB}(\mathbf{p})}$ .

# IV. NUMERICAL RESULTS

The proposed cooperative ML estimation framework is validated through numerical simulation, varying the number of BSs,  $N_{\rm bs}$ , up to 3, in the scenario shown in Fig. 1 with system parameters listed in Table I. Additionally, cooperative ML estimation performance is compared against (a) a single-BS setup, where localization relies on local range and angle estimates, and (b) cooperative localization based on least squares (LS). For LS, following the linearization of the relationship between range and the target position, as described in [17], a system of linear equations is formed by incorporating both AoA and range estimates collected from each BS. The LS solution is then obtained according to [18, Equation (20)], with range replacing RSS measurements and  $\mathbf{W} = \mathbf{I}_{2N_{\rm bs}-1}$ , where  $2N_{\rm bs}-1$  is the number of equations. The three BSs

<sup>&</sup>lt;sup>3</sup>The number of targets and their RoIs can be determined through target detection methods, such as generalized likelihood ratio test (GLRT) or constant false alarm rate (CFAR) detectors (see [14] and references therein).

<sup>&</sup>lt;sup>4</sup>As can be seen by substituting (16) into (15), solving (15) requires computing the partial derivatives of  $\Psi$ , whose closed-form expressions can be found in [11].

are numbered as in Fig. 1 and placed at the corners of a square area with a side length of  $85\,\mathrm{m}$ , with the origin of the common reference system in  $\mathcal{O}_1$ . The following rotation angles,  $[\vartheta_1,\vartheta_2,\vartheta_3]=[\pi/4,5\pi/4,3\pi/4]$ , are considered. The point-like target moves along the diagonal connecting BS<sub>1</sub> and BS<sub>2</sub>.<sup>5</sup> As outlined in Section III-B, a two-stage estimation, consisting of a coarse and a refined estimation within a defined RoI, is performed. For the coarse estimation, the search steps  $\delta f_\mathrm{D},\ \delta \tau,\ \delta \phi$  are computed with  $c_\tau=1,\ c'_{f_\mathrm{D}}=c'_\phi=0.25,$  with  $\Delta\Phi\simeq0.1108\,\mathrm{rad}$ . The matrix  $\Psi$  used to compute G in (10) and (14) is calculated based on the approximation method illustrated in [11], specifically using  $N_\mathrm{lobe}=5$  with reference to [11, Equation (44)].

Sensing performance is evaluated in terms of RMSE of range, angle, and position estimates. For a given vector of parameters q, this is computed as RMSE  $\sqrt{\frac{1}{N_{\rm MC}}\sum_{m=1}^{N_{\rm MC}}\|\hat{\mathbf{q}}_m-\mathbf{q}\|^2}$ , being  $N_{\rm MC}=500$  the number of Monte Carlo iterations. The results are shown in Fig. 2, where RMSEs alongside the corresponding CRLBs are plotted against varying target's position. Since the target moves along the square's diagonal y = x, its position in the common reference system is represented here by its x coordinate only. Fig. 2a and Fig. 2b show the RMSEs of range and angle estimates for single-BS scenarios. Additionally, the blue curve in Fig. 2c provides the position estimation RMSE when BS<sub>1</sub> operates alone. These results highlight the limitations of single-BS localization, where position RMSE can reach up to 1.34 m. Conversely, Fig. 2c demonstrates the benefits of cooperative ML position estimation, which outperforms both the single-BS scenario and the LS solution, particularly in low signal-to-noise ratio regions for at least one BS. For  $N_{\rm bs} \geq 2$ , position RMSE is at most 0.3 m and 0.1 m with two and three BSs, respectively, compared to 0.9 m and 0.7 m with LS. As a further example, when  $x = 54.2 \,\mathrm{m}$ , the RMSE is 0.98 m, 0.16 m, and 0.097 m for 1, 2, and 3 BSs, respectively, while for the LS, it is 0.50 m and 0.22 m with 2 and 3 BSs, respectively. Notably, for the considered single-target scenario, the proposed cooperative ML framework achieves performance that closely matches the corresponding PEB, underscoring the effectiveness of cooperative ML estimation.

# V. CONCLUSION

This letter proposed a cooperative ML framework for target position estimation in MIMO OTFS-based ISAC networks with multiple cooperating monostatic BSs. Results demonstrated the significant advantages of inter-BS cooperation: specifically, the cooperative approach achieved a position estimation error below 10 cm with three BSs, a sevenfold improvement over single BS configurations. Furthermore, the proposed framework closely approached the theoretical PEB, underscoring its efficiency.

#### APPENDIX

Considering a given BS and omitting its index i, after a few manipulations, (8) takes on the form

$$l(\mathbf{y}; \boldsymbol{\theta}, \mathbf{x}) \approx -\frac{1}{\sigma_{\nu}^2} \left( \beta^2 \left\| \mathbf{G} \mathbf{x} \right\|^2 + \left\| \mathbf{y} \right\|^2 - 2\beta \Re \mathfrak{e} \{ e^{j\varphi} \mathbf{y}^{\mathsf{H}} \mathbf{G} \mathbf{x} \} \right).$$

Now, ignoring those constant positive terms that do not contribute to the estimation, the log-likelihood reduces to

$$\tilde{l}(\mathbf{y}; \boldsymbol{\theta}, \mathbf{x}) = 2\beta \Re \{e^{j\varphi} \mathbf{y}^{\mathsf{H}} \mathbf{G} \mathbf{x}\} - \beta^2 \|\mathbf{G} \mathbf{x}\|^2.$$
 (18)

From (18) the vector of unknown parameters  $\theta$  can be estimated by maximizing the log-likelihood as

$$\widehat{\boldsymbol{\theta}}_{\mathrm{ML}} = \underset{[\beta, \varphi, f_{\mathrm{D}}, \tau, \phi]}{\arg \max} \ \widetilde{l}(\mathbf{y}; \boldsymbol{\theta}, \mathbf{x}). \tag{19}$$

Since  $\beta > 0$ , the phase  $\varphi$  of the complex channel coefficient h that maximizes  $\tilde{l}(\mathbf{y}; \boldsymbol{\theta}, \mathbf{x})$  is  $\hat{\varphi} = -\angle \mathbf{y}^{\mathsf{H}} \mathbf{G} \mathbf{x}$  and by replacing it in (18), this can be rewritten as

$$\tilde{l}(\mathbf{y}; \boldsymbol{\theta}, \mathbf{x}) = 2\beta |\mathbf{y}^{\mathsf{H}} \mathbf{G} \mathbf{x}| - \beta^2 ||\mathbf{G} \mathbf{x}||^2.$$
 (20)

The value of  $\beta$  which maximizes the likelihood function can be easily obtained and used for  $\hat{h} = \hat{\beta}e^{j\hat{\phi}}$ , as follows

$$\widehat{\beta} = \frac{|\mathbf{y}^{\mathsf{H}}\mathbf{G}\mathbf{x}|}{\|\mathbf{G}\mathbf{x}\|^2}, \qquad \widehat{h} = \frac{\mathbf{x}^{\mathsf{H}}\mathbf{G}^{\mathsf{H}}\mathbf{y}}{\|\mathbf{G}\mathbf{x}\|^2}.$$
 (21)

Lastly, by plugging  $\widehat{\beta}$  into (20), solving (19) reduces to

$$\left[\widehat{f}_{D}, \widehat{\tau}, \widehat{\phi}\right] = \underset{\left[f_{D}, \tau, \phi\right] \in \mathbb{R}^{3}}{\arg \max} \frac{|\mathbf{y}^{\mathsf{H}} \mathbf{G} \mathbf{x}|^{2}}{\left\|\mathbf{G} \mathbf{x}\right\|^{2}}.$$
 (22)

# REFERENCES

- [1] Z. Wei *et al.*, "Integrated sensing and communication enabled multiple base stations cooperative sensing towards 6G," *IEEE Network*, vol. 38, no. 4, pp. 207–215, Jul. 2024.
- [2] Y. Xu, L. Xie, D. Xu, and S. Song, "Fundamental limits and base station selection for collaborative sensing in perceptive mobile networks," in Proc. IEEE Int. Mediterranean Conf. on Commun. and Netw. (Medit-Com), Dubrovnik, Croatia, Sep. 2023, pp. 97–102.
- [3] Z. Wei et al., "Symbol-level integrated sensing and communication enabled multiple base stations cooperative sensing," *IEEE Trans. Veh. Technol.*, vol. 73, no. 1, pp. 724–738, Jan. 2024.
- [4] P. Gao, L. Lian, and J. Yu, "Cooperative ISAC with direct localization and rate-splitting multiple access communication: A pareto optimization framework," *IEEE J. Sel. Areas Commun.*, vol. 41, no. 5, pp. 1496–1515, May 2023.
- [5] M. Chen et al., "Joint node selection and resource allocation optimization for cooperative sensing with a shared wireless backhaul," 2024. [Online]. Available: https://arxiv.org/abs/2405.16791
- [6] K. Meng and C. Masouros, "Cooperative sensing and communication for ISAC networks: Performance analysis and optimization," in *Proc. IEEE Work. Signal Proc. Adv. Wirel. Comm. (SPAWC)*, Lucca, Italy, Sep. 2024, pp. 446–450.
- [7] L. Gaudio, M. Kobayashi, G. Caire, and G. Colavolpe, "On the effectiveness of OTFS for joint radar parameter estimation and communication," *IEEE Trans. Commun.*, vol. 19, no. 9, pp. 5951–5965, Sep. 2020.
- [8] M. Yağcıoğlu, "Dynamic resource allocation and interference coordination for millimeter wave communications in dense urban environment," Trans. Emerg. Telecommun. Technol., vol. 33, no. 5, May 2022.
- [9] B. Friedlander, "On transmit beamforming for MIMO radar," *IEEE Trans. Aerosp. Electron. Syst.*, vol. 48, no. 4, pp. 3376–3388, Oct. 2012.
- [10] R. Hadani et al., "Orthogonal time frequency space modulation," CoRR, vol. abs/1808.00519, 2018. [Online]. Available: http://arxiv.org/abs/1808.00519
- [11] T. Bacchielli, L. Pucci, E. Paolini, and A. Giorgetti, "A low-complexity detector for OTFS-based sensing," *IEEE Trans. Wireless Commun.*, Mar. 2025.

 $<sup>^5</sup> This$  trajectory illustrates the benefits of cooperative localization, as the target experiences varying distances to  $BS_1$  while progressively benefiting from  $BS_2$  and  $BS_3$ . The advantages demonstrated here apply to any trajectory within the monitored area.

- [12] S. K. Dehkordi et al., "Beam-space MIMO radar for joint communication and sensing with OTFS modulation," IEEE Trans. Wireless Commun., vol. 22, no. 10, pp. 6737–6749, Oct. 2023.
- [13] ——, "Multistatic parameter estimation in the near/far field for integrated sensing and communication," *IEEE Trans. Wireless Commun.*, vol. 23, no. 12, pp. 17929–17944, Dec. 2024.
  [14] M. Xu *et al.*, "CFAR based NOMP for line spectral estimation and
- [14] M. Xu et al., "CFAR based NOMP for line spectral estimation and detection," *IEEE Trans. Aerosp. Electron. Syst.*, vol. 59, no. 5, pp. 6971– 6990, Oct. 2023.
- [15] Y. Shen and M. Z. Win, "Fundamental limits of wideband localization—part I: A general framework," *IEEE Trans. Inf. Theory*, vol. 56, no. 10,
- pp. 4956-4980, Sep. 2010.
- [16] L. Pucci and A. Giorgetti, "Position error bound for cooperative sensing in MIMO-OFDM networks," in *Proc. IEEE Work. Signal Proc. Adv. Wirel. Comm. (SPAWC)*, Lucca, Italy, Sep. 2024, pp. 296–300.
- [17] M. Pelka, "Position calculation with least squares based on distance measurements," Lübeck University of Applied Sciences, Tech. Report, 2015. [Online]. Available: http://www.th-luebeck.de
- [18] W. Ding, S. Chang, and S. Bao, "A simple and efficient RSS-AOA based localization with heterogeneous anchor nodes," 2023. [Online]. Available: https://arxiv.org/abs/2307.11951